Roman Kostecki, Heike Ebendorff-Heidepriem, Stephen C. Warren-Smith, and Tanya M. Monro

Predicting the drawing conditions for microstructured optical fiber fabrication

Optical Materials Express, 2014; 4(1):29-40

Predicting the Drawing Conditions for Microstructured Optical Fiber Fabrication

Roman Kostecki*, Heike Ebendorff-Heidepriem, Stephen C. Warren-Smith, and Tanya M. Monro

Institute for Photonics and Advanced Sensing and School of Chemistry and Physics, The University of Adelaide, Adelaide, South Australia 5005, Australia

*roman.kostecki@adelaide.edu.au

Abstract: The efficient and accurate fabrication of Microstructured optical fibers (MOFs) requires a practical understanding of the 'draw process' beyond what is achievable by trial and error, which requires the ability to predict the experimental drawing parameters needed to produce the desired final geometry. Our results show that the Fitt *et al.* fluid-mechanics model for describing the draw process of a single axisymmetric capillary fiber provides practical insights when applied to more complex multi-hole symmetric and asymmetric MOF geometries. By establishing a method to relate the multi-hole MOF geometry to a capillary and understanding how material temperature varies with the draw tower temperature profile, it was found that analytical equations given by the Fitt model could be used to predict the parameters necessary for the chosen structure. We show how this model provides a practical framework that contributes to the efficient and accurate fabrication of the desired MOF geometries by predicting suitable fiber draw conditions.

OCIS codes: (060.2280) Fiber design and fabrication; (060.2290) Fiber materials; (060.2310) Fiber optics; (060.4005) Microstructured fibers; (080.2720) Mathematical methods (general); (220.4000) Microstructure fabrication; (350.3850) Materials processing; (350.4600) Optical engineering

References and links

1. P. Kasier, E. A. J. Marcatili, and S. E. Miller, "A new optical fiber," Bell Sys. Tech. J. **52**, 265 – 269 (1973).
2. J. C. Knight, T. A. Birks, P. S. J. Russell, and D. M. Atkin, "All-silica single-mode optical fiber with photonic crystal cladding," Opt. Lett. **21**, 1547 – 1549 (1996).
3. T. M. Monro and H. Ebendorff-Heidepriem, "Progress in microstructured optical fibers," Annu. Rev. Mater. Res. **36**, 467 – 495 (2006).
4. W. Q. Zhang, H. Ebendorff-Heidepriem, T. M. Monro, and S. Afshar V., "Fabrication and supercontinuum generation in dispersion flattened bismuth microstructured optical fiber," Opt. Express **19**, 21135 – 21144 (2011).
5. M. Oermann, H. Ebendorff-Heidepriem, D. Ottaway, D. Lancaster, P. Veitch, and T. Monro, "Extruded microstructured fiber lasers," IEEE Photon. Technol. Lett. **24**, 578 – 580 (2012).
6. S. Atakaramians, S. Afshar V., H. Ebendorff-Heidepriem, M. Nagel, B. M. Fischer, D. Abbott, and T. M. Monro, "THz porous fibers: design, fabrication and experimental characterization," Opt. Express **17**, 14053 – 15062 (2009).
7. N. A. Issa, "High numerical aperture in multimode microstructured optical fibers," Appl. Opt. **43**, 6191 – 6197 (2004).
8. B. Gauvreau, F. Desevedavy, N. Guo, D. Khadri, A. Hassani, and M. Skorobogatiy, "High numerical aperture polymer microstructured fiber with three super-wavelength bridges," J. Opt. A. – Pure Appl. Op. **11**, 085102 (2009).

9. T. M. Monro, D. J. Richardson, and P. J. Bennett, "Developing holey fibres for evanescent field devices," Electron. Lett. **35**, 1188 – 1189 (1999).
10. O. S. Wolfbeis, "Fiber-optic chemical sensors and biosensors," Anal. Chem. **80**, 4269 – 4283 (2008).
11. T. M. Monro, S. Warren-Smith, E. P. Schartner, A. François, S. Heng, H. Ebendorff-Heidepriem, and S. Afshar V., "Sensing with suspended-core optical fibers," Opt. Fiber Technol. **16**, 343 – 356 (2010).
12. S. Heng, M.-C. Nguyen, R. Kostecki, T. M. Monro, and A. D. Abell, "Nanoliter-scale, regenerable ion sensor: sensing with a surface functionalized microstructured optical fibre," RSC Adv. **3**, 8308 – 8317 (2013).
13. K. Mukasa, K. Imamura, M. Takahashi, and T. Yagi, "Development of novel fibers for telecoms application," Opt. Fiber Technol. **16**, 367 – 377 (2010).
14. H. Ebendorff-Heidepriem and T. M. Monro, "Extrusion of complex preforms for microstructured optical fibers," Opt. Express **15**, 15086 – 15092 (2007).
15. H. Ebendorff-Heidepriem and T. M. Monro, "Analysis of glass flow during extrusion of optical fiber preforms," Opt. Mater. Express **2**, 304 – 320 (2012).
16. Y. Zhu, R. T. Bise, J. Kanka, P. Peterka, and H. Du, "Fabrication and characterization of solid-core photonic crystal fiber with steering-wheel air-cladding for strong evanescent field overlap," Opt. Commun. **281**, 55 – 60 (2008).
17. H. E. Hamzaoui, L. Bigot, G. Bouwmans, I. Razdobreev, M. Bouazaoui, and B. Capoen, "From molecular precursors in solution to microstructured optical fiber: a sol-gel polymeric route," Opt. Mater. Express **1**, 234 – 242 (2011).
18. A. S. Webb, F. Poletti, D. J. Richardson, and J. K. Sahu, "Suspended-core holey fiber for evanescent-field sensing," Opt. Eng. **46** (2007).
19. P. McNamara, D. Lancaster, R. Bailey, A. Hemming, P. Henry, and R. Mair, "A large core microstructured fluoride glass optical fibre for mid-infrared single-mode transmission," J. Non-Cryst. Solids **355**, 1461 – 1467 (2009).
20. J. Lægsgaard and A. Bjarklev, "Microstructured optical fibers – fundamentals and applications," J. Am. Ceram. Soc. **89**, 2 – 12 (2006).
21. A. D. Pryamikov, A. S. Biriukov, A. F. Kosolapov, V. G. Plotnichenko, S. L. Semjonov, and E. M. Dianov, "Demonstration of a waveguide regime for a silica hollow - core microstructured optical fiber with a negative curvature of the core boundary in the spectral region $> 3.5\ \mu$m," Opt. Express **19**, 1441 – 1448 (2011).
22. S. E. Rosenberg, H. Papamichael, and I. N. Miaoulis, "A 2-dimensional analysis of the viscous problem of a glass preform during the optical-fiber drawing process," Glass Technol. **35**, 260 – 264 (1994).
23. A. Mawardi and R. Pitchumani, "Optical fiber drawing process model using an analytical neck-down profile," IEEE Photon. J. **2**, 620 – 629 (2010).
24. S. C. Xue, R. I. Tanner, G. W. Barton, R. Lwin, M. C. J. Large, and L. Poladian, "Fabrication of microstructured optical fibers – Part 1 & 2," J. Lightwave Technol. **23**, 2245 – 2266 (2005).
25. G. Luzi, P. Epple, M. Scharrer, K. Fujimoto, C. Rauh, and A. Delgado, "Influence of surface tension and inner pressure on the process of fibre drawing," J. Lightwave Technol. **28**, 1882 – 1888 (2010).
26. A. D. Fitt, K. Furusawa, T. M. Monro, C. P. Please, and D. J. Richardson, "The mathematical modelling of capillary drawing for holey fibre manufacture," J. Eng. Math. **43**, 201 – 227 (2002).
27. R. Kostecki, H. Ebendorff-Heidepriem, C. Davis, G. McAdam, S. C. Warren-Smith, and T. M. Monro, "Silica exposed-core microstructured optical fibers," Opt. Mater. Express **2**, 1538 – 1547 (2012).
28. S. H. K. Lee and Y. Jaluria, "Simulation of the transport processes in the neck-down region of a furnace drawn optical fiber," Int. J. Heat Mass Tran. **40**, 843 – 856 (1997).
29. R. M. Wynne, "A fabrication process for microstructured optical fibers," J. Lightwave Technol. **24**, 4304 – 4313 (2006).
30. C. Voyce, A. Fitt, and T. Monro, "Mathematical model of the spinning of microstructured fibres," Opt. Express **12**, 5810 – 5820 (2004).
31. C. J. Voyce, A. D. Fitt, and T. M. Monro, "The mathematical modelling of rotating capillary tubes for holey-fibre manufacture," J. Eng. Math. **60**, 69 – 87 (2008).
32. C. J. Voyce, A. D. Fitt, and T. M. Monro, "Mathematical modeling as an accurate predictive tool in capillary and microstructured fiber manufacture: The effects of preform rotation," J. Lightwave Technol. **26**, 791 – 798 (2008).
33. C. J. Voyce, A. D. Fitt, J. R. Hayes, and T. M. Monro, "Mathematical modeling of the self-pressurizing mechanism for microstructured fiber drawing," J. Lightwave Technol. **27**, 871 – 878 (2009).
34. G. Luzi, P. Epple, M. Scharrer, K. Fujimoto, C. Rauh, and A. Delgado, "Asymptotic analysis of flow processes at drawing of single optical microfibres," Int J. Chem. Reactor Eng. **9** (2011).
35. U. C. Paek and R. B. Runk, "Physical behavior of the neck-down region during furnace drawing of silica fibers," J. Appl. Phys. **49**, 4417 – 4422 (1978).
36. G. Yang, T. Rouxel, J. Troles, B. Bureau, C. Boussard-Plèdel, P. Houizot, and J.-C. Sangleboeuf, "Viscosity of As_2Se_3 glass during the fiber drawing process," J. Am. Ceram. Soc. **94**, 2408 – 2411 (2011).
37. K. Richardson, D. Krol, and K. Hirao, "Glasses for photonic applications," Int. J. Appl. Glass Sci. **1**, 74 – 86 (2010).
38. M.-J. Li and D. A. Nolan, "Optical transmission fiber design evolution," J. Lightwave Technol. **26**, 1079 – 1092 (2008).

39. Heraeus Quarzglas GmbH & Co. KG, http://heraeus-quarzglas.com/, *Pure Silica Rods for Specialty Fiber Applications*, 01st ed. (2012).
40. E. P. Schartner, H. Ebendorff-Heidepriem, S. C. Warren-Smith, R. T. White, and T. M. Monro, "Driving down the detection limit in microstructured fiber-based chemical dip sensors," Sensors **11**, 2961 – 2971 (2011).
41. R. Kostecki, E. P. Schartner, H. Ebendorff-Heidepriem, P. C. Henry, and T. M. Monro, "Fabrication of suspended and exposed core silica fibres for sensing applications," ACOFT - 37th Australian Conference on Optical Fibre Technology (2012).
42. G. Urbain, Y. Bottinga, and P. Richet, "Viscosity of liquid silica, silicates and alumino-silicates," Geochim. Cosmochim. Ac. **46**, 1061 – 1072 (1982).
43. R. H. Doremus, "Viscosity of silica," J. Appl. Phys. **92**, 7619 – 7629 (2002).
44. S. Roy Choudhury and Y. Jaluria, "Thermal transport due to material and gas flow in a furnace for drawing an optical fiber," J. Mater. Res. **13**, 494 – 503 (1998).
45. N. M. Parikh, "Effect of atmosphere on surface tension of glass," J. Am. Ceram. Soc. **41**, 18 – 22 (1958).
46. W. D. Kingery, "Surface tension of some liquid oxides and their temperature coefficients," J. Am. Ceram. Soc. **42**, 6 – 10 (1959).
47. K. Boyd, H. Ebendorff-Heidepriem, T. M. Monro, and J. Munch, "Surface tension and viscosity measurement of optical glasses using a scanning CO_2 laser," Opt. Mater. Express **2**, 1101 – 1110 (2012).
48. A. D. Fitt, K. Furusawa, T. M. Monro, and C. P. Please, "Modeling the fabrication of hollow fibers: capillary drawing," J. Lightwave Technol. **19**, 1924 – 1931 (2001).
49. H. Ebendorff-Heidepriem, S. C. Warren-Smith, and T. M. Monro, "Suspended nanowires: fabrication, design and characterization of fibers with nanoscale cores," Opt. Express **17**, 2646 – 2657 (2009).
50. R. Kostecki, H. Ebendorff-Heidepriem, S. C. Warren-Smith, G. McAdam, C. Davis, and T. M. Monro, "Optical fibres for distributed corrosion sensing – architecture and characterisation," Key Eng. Mat. **558**, 522 – 533 (2013).
51. S. C. Warren-Smith, H. Ebendorff-Heidepriem, T. C. Foo, R. Moore, C. Davis, and T. M. Monro, "Exposed-core microstructured optical fibers for real-time fluorescence sensing," Opt. Express **17**, 18533 – 18542 (2009).

1. Introduction

Microstructured optical fibers [1] (MOFs) are an important class of fiber often with longitudinal air holes that provide a large refractive index contrast used for light confinement [2]. Unlike conventional optical fibers, MOFs with air holes can be manufactured from a single material, and with the appropriate cross-sectional design, the structure can provide a broad range of highly unusual and tailorable optical properties [3]. By the suitable selection of glass or polymer material and geometry the dispersion, nonlinearity, birefringence, polarization, evanescent field and mode area of the propagating light can be optimized to specific applications. This has led to innovations in supercontinuum generation [4], fiber lasers [5], terahertz wave guiding [6], fibers with high numerical apertures [7, 8], sensors [9–12], and makes MOFs an excellent candidate for new high-capacity transmission multicore and endlessly single mode telecommunications fibers [13].

All optical fibers are produced by heating and drawing down a preform from an initial diameter of the order of centimeters to the desired final diameter using a fiber drawing tower. For MOFs with longitudinal air holes this draw process includes a mechanism by which the pressure difference of the holes and atmosphere is maintained to ensure the holes collapse or expand to the desired final geometry. Some common ways to produce MOF preforms include using extrusion [14, 15], sol-gel casting [16, 17], ultrasonic drilling [18, 19] or stack and draw methods [2, 20, 21], which resemble a large-scale form of the final desired fiber geometry. The fiber drawing tower is then used to feed the preform at a fixed rate into a furnace, which heats the material to an appropriate viscosity, so it can taper down to the final fiber diameter (usually of the order of hundreds of micrometers) by drawing the fiber below the furnace at a faster rate. The extensive range of possibilities means that in order to fabricate MOFs in an efficient manner, it is essential that these draw conditions can be predicted accurately.

It is not the intention of this paper to describe the draw process of MOFs, as this has already been done by several studies [22–25]. Instead, we describe how the analytical model provided by Fitt *et al.* [26] can be used to predict suitable fiber draw conditions when applied to multi-hole MOF geometries. This model, describing the process of a single axisymmetric hole fiber,

was shown to give excellent agreement to a range of capillary drawing experiments, providing practical guidelines useful in the design and control of capillary fabrication [26]. The results shown in this paper provide experimental validation of the ability for the Fitt model to predict the parameters needed for fabrication of symmetric and asymmetric multi-hole fiber structures. In particular, we show the predictive nature of this model when applied to fabrication of three hole symmetric suspended-core fiber [18] and two hole asymmetric exposed-core fibers [27]. The advantages of having analytic equations for the fiber draw process are these equations allow prediction of processing parameters such as temperature and pressure to achieve desired final MOF geometries. This avoids the need for systematic scanning of drawing parameters such as temperature and pressure during the fiber draw. Given that each time the drawing conditions are changed it takes time for the draw process to stabilize, which reduces the fiber yield possible from the preform. Such equations can also provide insight into the nature of the process.

2. The MOF draw process

In theory, the set of Navier-Stokes coupled differential equations can be used to describe the neck down region viscous fluid flow of the MOF draw process to model the shape of the final expected fiber geometry [22,23]. These equations describe how the velocity, pressure, temperature, and density of a moving fluid are related as well as how these quantities are transferred inside the physical system due to diffusion and convection. Solving these equations for MOF production becomes a tedious numerical problem due to the large set of parameters involved in the fiber draw process. To overcome this, suitable approximations and generalizations have been studied in order to develop useful draw process predictive models [24].

In 2002, starting from the Navier-Stokes and convection-diffusion equations, Fitt *et al.* [26] derived and experimentally validated a general model describing the draw process of a capillary (Fitt model), which is capable of including the effects of internal hole pressurization, surface tension and all of the other effects useful for predicting the draw process. The Fitt model assumes that viscosity alone is a function of temperature, ignoring some of the weak dependance [28] that temperature has on physical quantities such as material density, surface tension, thermal conductivity and specific heat, since the material viscosity typically varies by orders of magnitude over a relatively modest temperature range. Also, although the Fitt model accounts for physical effects such as diffusive and convective heat transfer, some simplifications are made where the terms in the equations are small, such as ignoring viscous dissipation, and that the optically thin fiber absorbs radiation directly from the surrounding furnace and re-radiates heat back to the furnace. With these approximations and appropriate choice of practical boundary conditions for fiber drawing purposes, a set of analytical equations for the case of a capillary was developed.

There have been several studies utilizing the methods described by Fitt *et al.* [26], such as models to; determine the drawing domain of internal hole pressurization when applied to a square lattice geometry [29], include the effects of preform rotation [30–32] and self pressurization [33], and asymptotic analysis of surface tension and internal hole pressurization affects on the drawing process [34]. In this paper we demonstrate how the Fitt model can be used as a practical predictive tool to produce multi-hole symmetric and asymmetric fiber structures, and provides the first experimental validation of these analytical equations when applied to MOFs rather than simple capillaries.

2.1. Fitt model

The Fitt model equation describing the internal diameter (h_1 [m]) of a single axisymmetric hole fiber, is given by [26],

$$h_1(p_0) = \exp\left(\frac{-\beta z}{2L} - P\exp\left(\frac{-\beta z}{L}\right)\right)\left[h_{10}\exp(P) - G\int_0^z \exp\left(\frac{-\beta u}{2L} + P\exp\left(\frac{-\beta u}{L}\right)\right)\mathrm{d}u\right]$$

$$G = \frac{\gamma}{2\mu W_f} \quad , \quad P = \frac{p_0 L}{2\beta\mu W_f} \quad , \quad \beta = \ln\left(\frac{W_d}{W_f}\right) \tag{1}$$

where, μ [Pa.s] denotes the viscosity, p_0 [Pa] denotes internal hole overpressure (above atmospheric pressure), W_f [ms^{-1}] denotes the feeding speed for the preform, W_d [ms^{-1}] denotes the drawing speed for the fiber, z [m] denotes the distance along the axis from the start of the neck down region, γ [Nm^{-1}] denotes surface tension, and the heating zone length L [m] denotes the neck down region [35, 36]. This heating zone length is defined by Eq. (1) as the neck down region where the changes are integrated over $0 \leq z \leq L$ for the drawn fiber case.

2.2. Materials and equipment

High purity fused silica known as Suprasil F300HQ (Heraeus Quarzglas GmbH & Co.KG) was chosen for experiments. Silica is known to be reliable under a range of processing and use environments, with relatively better mechanical and thermal stability [37]. Highly homogeneous, high purity bulk material is commercially available, which has led to silica telecom fibers regularly being made with low loss ($\sim$0.2 dB/km at NIR wavelengths) [38]. This inherent low loss and relatively low intrinsic nonlinearity makes silica excellent for low or high power fiber applications, with a transmission window from UV to NIR (0.19–2.0 μm) [39]. Also, silica has a relatively low refractive index, which can improve the sensitivity of evanescent field sensors, since reducing the index contrast (Δn) at the core-cladding boundary increases the power fraction to the analyte or functionalized surface [40].

100 mm long fiber preforms were fabricated from Ø12 mm and Ø20 mm F300HQ silica rod, which were drilled with three Ø2.9 mm holes, where the centers of the holes form an equilateral triangle with 3.2 mm sides, and cleaned using the method discussed in Ref. [27]. Drilling was chosen since it has been demonstrated to be a relatively simple method for three hole structures [18] compared to the more widely used stacking method, and after cleaning the surface quality is satisfactory to produce fibers with relatively low losses [41]. The only difference between symmetric suspended-core fiber and asymmetric exposed-core fiber preforms, is that for the exposed-core fiber case a thin slot was cut into the side of the symmetric preform in order to expose the core region [27]. To draw the preform to fiber a 6 m tower with graphite resistance furnace, positive pressurization system and automated diameter control was used.

2.3. Temperature dependence of viscosity and surface tension

Knowing the temperature dependence of material viscosity is a major part of practically applying a model to the fiber drawing process. For F300 silica in the temperature range 1673 K $\leq T \leq$ 2773 K the viscosity, experimentally measured by Urbain *et al.* [42] and discussed by Doremus [43] and Voyce *et al.* [32], is given by,

$$\mu = 5.8\times10^{-8}\exp\left(\frac{515400}{RT}\right) \quad \text{[Pa.s]} \tag{2}$$

where R is the gas constant and T [K] is the glass temperature. In order to find closed form solutions of Eq. (1) it is necessary that the temperature of the glass is assumed constant. However, a drawing tower furnace does not exhibit a constant temperature but an axial temperature

gradient/profile [32, 36]. This means that the glass viscosity varies with the temperature gradient/profile within the furnace [44]. One should also consider that temperature profiles can vary between drawing towers and furnace designs.

To determine the temperature profile inside the preform for the conditions prevailing within our draw tower, a thermocouple was inserted in the center of a drilled F300HQ silica glass rod. The measurements of the thermocouple temperature were taken for Ø12 mm and Ø20 mm rods at 5 mm intervals along the central axis of the furnace, ensuring thermal equilibrium at each measured point. For furnace temperature measurements, the draw tower was equipped with a pyrometer located next to a furnace element and targeted at the inner sleeve of the furnace. Figure 1(a) shows the results of the thermocouple temperatures measured at 1500 °C, 1600 °C, and 1700 °C furnace temperatures, shown in blue, green and orange respectively, where the small and large dots correspond to the measured points for the Ø12 mm and Ø20 mm rods respectively. The three furnace temperatures were chosen so the results could be extrapolated to typically higher fiber drawing temperatures.

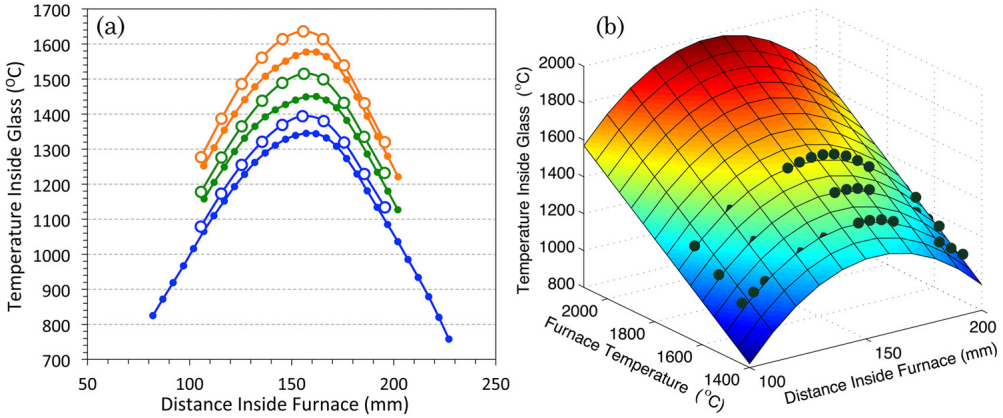

Fig. 1. (a) Temperature profiles measured inside (small dots) Ø12 mm and (large dots) Ø20 mm rods at (blue) 1500 °C, (green) 1600 °C, and (orange) 1700 °C furnace temperatures. (b) Surface of 2×1 degree polynomial (Eq. (3)) fitted to the Ø12 mm results shown by green dots. The distance inside furnace was measured from the top of the furnace outer casing.

These temperature profile results show that the temperature measured inside the silica glass rod is lower for smaller diameters. Larger diameter preforms are closer to the surrounding heating element, placing the outside of the glass in a hotter part of the furnace [44], which results in a hotter temperature inside the preform and shows the role that glass thermal conductivity has in the heat transfer process. For the three Ø12 mm silica rod temperature profiles, the 2×1 degree polynomial given by,

$$T_{\mathrm{m}} = -3634 + 43.71\,\xi + 1.073\,T_{\mathrm{f}} - 0.1416\,\xi^2 - 2.404\times10^{-5}\,\xi\,T_{\mathrm{f}} \tag{3}$$

fits the curves with R^2 of 0.9899, where T_{m} is the measured temperature, T_{f} is the furnace temperature, and ξ is the distance inside the furnace from top of the outer casing. The surface given by Eq. (3) is shown in Fig. 1(b) together with the three sets of measured points. Similarly, for the three Ø20 mm silica rod temperature profiles, the 2×1 degree polynomial given by,

$$T_{\mathrm{m}} = -4704 + 51.79\,\xi + 1.537\,T_{\mathrm{f}} - 0.1551\,\xi^2 - 2.201\times10^{-3}\,\xi\,T_{\mathrm{f}} \tag{4}$$

fits the curves with R^2 of 0.9957.

For calculations shown in this paper, the surface tension of silica is assumed constant at 0.31 Nm^{-1} [45–47], since it varies weakly with temperature within the fiber drawing range.

2.4. Defining the geometry

The Fitt model describes a capillary draw process for which we define the geometry change during drawing as the ratio [48],

$$C = \frac{h_1 h_{20}}{h_2 h_{10}} \tag{5}$$

where h_{10} and h_{20} are the preform inner and outer diameters. This ratio provides a comparison of the final fiber geometry ratio (h_1/h_2) to the initial preform geometry ratio (h_{10}/h_{20}) of the inner and outer diameters. When $C = 1$ then the hole geometry is preserved. If $C > 1$ then the hole expands from the original geometry, and the hole experiences collapse when $C < 1$. With Eq. (1) and the external fiber diameter (h_2 [m]) given by [26],

$$h_2 = h_{20}\ \exp\left(\frac{-\beta}{2}\right) \quad , \tag{6}$$

Eq. (5) becomes,

$$C(p_0) = \frac{\exp\left(-P\exp\left(-\beta\right)\right)}{h_{10}} \left[h_{10}\exp(P) - G\int_0^z \exp\left(\frac{-\beta u}{2L} + P\exp\left(\frac{-\beta u}{L}\right)\right) \mathrm{d}u \right] \tag{7}$$

for the $z = L$ drawn fiber case. To obtain a closed form Eq. (7), Eq. (6) assumes that the draw down ratio (β) is independent of inner diameters, which can only be valid for small hole changes.

Since the geometry change ratio (C) describes a capillary draw process, a method to relate the geometry of a multi hole MOF to a capillary needed to be established. To measure the fabricated structures and calculate C according to Eq. (5), we chose to define the 'hole region diameter' of h_1 and h_{10} as being the diameter of a circle that has the same circumference as the total of all the inner hole perimeters. The outside diameters, h_2 and h_{20} were measured directly. This definition for the inner diameter was found to have a better correlation between Eq. (7) and experimental, compared to other definitions tried such as hydraulic diameter, or the diameter of a circle that fits tightly around the inner holes, or the diameter of a circle that has the same area as the total area of the inner holes.

3. Draw process experimental

3.1. Comparing the model with experiment

Two preforms were fabricated as discussed in Sec. 2.2 and shown in Fig. 4(a), and directly drawn down to fiber at Ø160 μm outside diameter. One of the preforms was used for a series of pressures and the other for a series of furnace temperatures, allowing enough time for the fiber structure to stabilize between each change which typically took approximately 5 minutes. In each case, a preform feed rate of 1.5 mm/min was used, and the draw tower was set to automatically maintain an appropriate draw speed to maintain the target outside diameter. Inner and outer diameters of each fiber structure from the series and the preforms were measured using images from a microscope and applying the definition discussed in Sec. 2.4. The neck down region length (L) was measured from the preforms after fiber drawing as being 0.039 m. Equation (5) was then used to calculate the value for the geometry change ratio (C), which are shown as the dots in Fig. 2. The temperature shown in Fig. 2(b) are the furnace temperatures, and the furnace temperature used for the pressure series (Fig. 2(a)) was 2000 °C.

As discussed in Sec. 2.3, although furnace temperature is known, it is not the actual glass temperature. We expected that the actual temperature of the glass in the neck down region to be less than the furnace temperature, due to axial and radial temperature gradients. Also, as discussed in Sec. 2 several assumptions were made in order to arrive at Eq. (1). It was therefore expected that not all of the contracting effects due to surface tension are completely accounted for in the Fitt model described in Sec. 2.1, which would lead to the actual internal hole overpressure (p_0) being different to the pressure measured by the draw tower control system (p_f). Because of these uncertainties, pressure (p_ε) and temperature (T_ε) offsets were included such that $p_0 = p_f + p_\varepsilon$ and $T = T_f + 273.15 + T_\varepsilon$, and fitted to the experimental data.

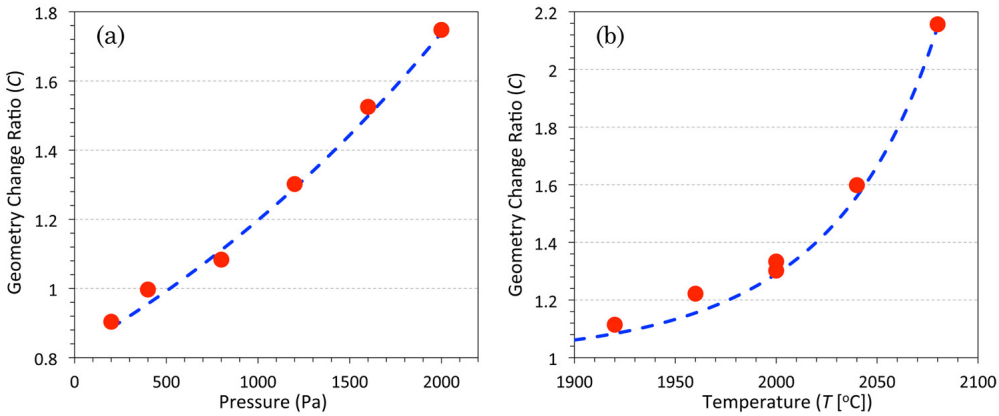

Fig. 2. Experimental (red dots) and model (blue line) for a series of pressures (a) and a series of furnace temperatures (b). For the pressure series (a) the furnace temperature used was 2000 °C at pressures of 200, 400, 800, 1200, 1600, and 2000 Pa. For the temperature series (b), furnace temperatures of 1920, 1960, 2000, 2040, and 2080 °C were used with a fixed pressure of 1200 Pa. The temperature series (b) also includes the 1200 Pa result from the pressure series.

It was found that by using fixed pressure and temperature offsets ($\pm$ 95% confidence interval) of $p_\varepsilon = -375.8 \pm 80.4$ Pa and $T_\varepsilon = -141.1 \pm 7.6$ K, Eq. (7) fits well with experiment with $R^2 = 0.9905$, as shown by the blue lines in Fig. 2. The peak temperature offset calculated from Eq. (3) at a furnace temperature of 2000 °C gives an offset of -123 °C, which is remarkably close to the value obtained for T_ε considering that only a step temperature profile is assumed in the model.

In Sec. 2.4, Eq. (6) assumes that the outside diameter (h_2) is independent of pressure, which leads to the geometry change ratio (Eq. (7)) being independent of outside diameter. It is interesting to compare this with the experimental results to verify if the assumptions are valid in this respect. The draw tower pressure and draw speed data obtained during the pressure series discussed above are shown in Fig. 3, where the blue line shows the pressure applied to the holes of the preform and the red line shows the draw speed. At the start of the experiment, where the automatic diameter control was switched off, a constant draw speed of 4 m/min was used while the pressure was switched on and allowed to stabilize to 200 Pa. The automatic diameter control was then switched on with a target outside diameter of 160 μm and the draw increased in speed until the target diameter was reached, at 8 m/min. As the pressure was increased to 400, 800 and 1200 Pa the draw speed did not increase, showing that within this range of hole expansion the outside diameter (h_2) of the final fiber is indeed independent of pressure. When the pressure was increased to 1.6 kPa the draw speed started to increase, as the automatic diameter con-

trol measured an increase in fiber diameter and increased the draw speed to compensate. After this initial increase, the draw speed reduced back towards the 8 m/min draw speed, showing that although the system experienced some instability there was tendency for the draw speed to remain constant. At the end of the fiber draw experiment the draw speed started to increase quickly, where the fiber draw is no longer in a steady state regime at the end of the preform.

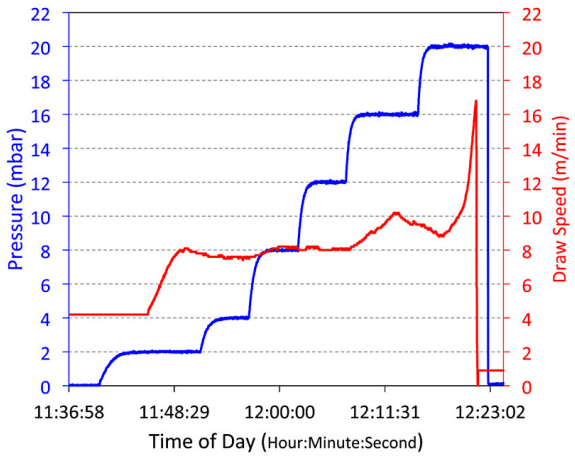

Fig. 3. Draw tower data, showing (blue) the pressure applied to the holes of the preform, and (red) the draw speed which was set to automatically maintain a constant outside fiber diameter.

These experimental results provide evidence that the assumptions made to arrive at Eq. (1) and Eq. (6) are within the range of pressures we used and for moderate geometry change ratios (up to $C \sim 2$), giving greater confidence in the Fitt model to predict the parameters which need to be considered for practical fiber drawing. The validation that the geometry change ratio (Eq. (7)) is independent of the MOFs outside diameter for moderate geometry change ratios leads to the proposition that it should be possible to create asymmetric structures where the cross sectional wall thickness surrounding the holes could be made non-axisymmetric.

3.2. Predicting fiber draw parameters

3.2.1. Suspended-core fibers: symmetric structures

The predictive nature of Eq. (7) is most useful for fabrication of MOFs. Equipped with the temperature and pressure offsets, our aim was to produce a fiber with a similar structure but smaller scale and core size, for which the cane and sleeve method [49] was required. The process is to first cane the preform to the order of millimeters, insert this cane into a rod (sleeve), and then draw down the cane and sleeve to fiber, which requires the successful application of the right combination of parameters in order to achieve the desired final fiber structure. Another preform was fabricated, as discussed in Sec. 2.2 and shown by Fig. 4(a), and drawn down to fiber using the cane and sleeve method.

For the cane, the feed rate needs to be greatly increased and the draw speed greatly reduced to achieve the lower draw down ratio. For this we chose a feed rate of 6.4 mm/min with the targeted outside diameter for the cane being Ø0.95 mm maximum. The aim was to pre-expand the holes during the caning process, for which we chose a geometry change ratio of $C = 1.55$. Using Eq. (7) the predicted pressure (p_f) needed to achieve this was 3.5 kPa at a furnace temperature of 1980 °C. A microscope image of the resulting cane structure is shown in Fig. 4(b), from which the outer diameter was measured as Ø0.91 mm with the hole region diameter Ø0.87 mm.

Applying the definition discussed in Sec. 2.4, the geometry change ratio (Eq. (5)) obtained for this cane was $C = 1.50$, which agrees well with the target $C = 1.55$.

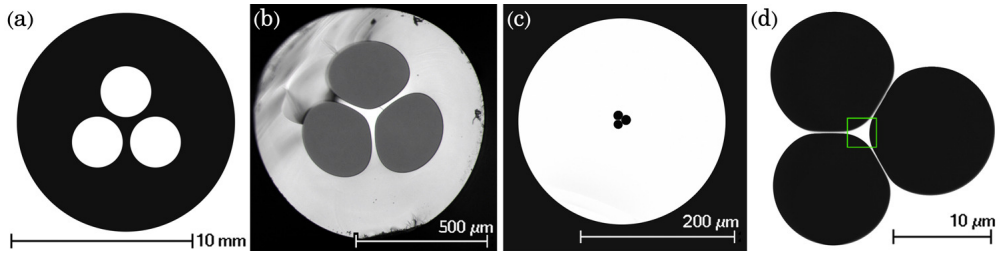

Fig. 4. (a) Cross section of the preform fabricated from Ø12 mm F300HQ silica rod; and, microscope image of (b) the cane; and, scanning electron microscope images of (c) the silica suspended-core fiber cross section measured to be Ø270 μm with (d) and enlarged image of the holes and core having effective diameters of 40.5 μm and 1.7 μm respectively.

A sleeve was made by drilling a Ø1 mm hole centrally located in Ø12 mm F300HQ silica rod into which the cane was placed. The setup of the cane and sleeve arrangement was made to ensure pressure was only applied to the three holes of the cane. The aim was to draw down the cane and sleeve to a suspended-core fiber with core size of Ø1.5-2.0 μm and target outside diameter of Ø270 μm. We chose a geometry change ratio of $C = 1.8$ to further expand the cane holes, for which Eq. (7) predicted the pressure (p_f) needed to achieve this was 2.7 kPa at a furnace temperature of 2000 °C and feed rate of 1.5 mm/min. A single 80 m long length of suspended-core fiber was fabricated using those parameters, as shown by the scanning electron microscope (SEM) images in Figs. 4(c)-4(d) from which the outer diameter was measured as being Ø270 μm with the hole region diameter Ø40.5 μm. Applying the definition discussed in Sec. 2.4, the geometry change ratio (Eq. (5)) obtained for this fiber was $C = 1.97$, which is $\sim$10% deviation from what was calculated by the model. The core, shown by the green box in Fig. 4(d), was measured as having a effective diameter of Ø1.7 μm, defined as the diameter of a circle whose area is equal to a triangle that fits wholly within the core area [49].

3.2.2. Exposed-core fibers: asymmetric structures

A preform was fabricated, as discussed in Sec. 2.2, with a 1.8 mm wide slot cut along the length of one hole in order to fabricate a fiber with the core exposed along the length. These types of exposed-core fibers are useful in sensing applications where real time measurements and/or emptying and re-filling is required, or long lengths are needed for distributed sensing applications [27]. The aim was to produce this type of asymmetric structure to a final maximum outside diameter of 200 μm, by directly drawing down the preform to fiber. Looking at the series of fibers discussed in Sec. 3.1, we chose to use a furnace temperature of 2000 °C and aimed to expand the holes in order to achieve a geometry change ratio of $C = 1.4$. Using Eq. (7) the predicted pressure (p_f) needed to achieve this was 1.40 kPa, at a preform feed rate of 1.5 mm/min. A single 127 m long uncoated exposed-core fiber (Fig. 5(a)) was fabricated using a pressure of 1.40 kPa and the outside was measured from SEM images as being Ø202 μm (measured at the maximum) with the hole region diameter of the two holes being Ø143.1 μm.

As shown in Fig. 5(a), the outside of this asymmetric structure no longer resembles the preform from which it was made (Fig. 4(a) with 1.8 mm slot). This is caused by surface tension increasing the initial gap provided by the 1.8 mm slot in the preform and significantly changing the geometry, adding a degree of complexity not accounted for in the Fitt model or in the way the geometry is defined (Sec. 2.4). Therefore, C was not calculated from measurements

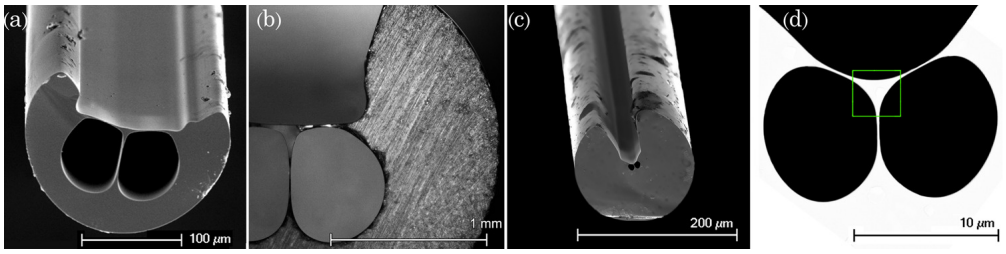

Fig. 5. Scanning electron microscope (SEM) image of (a) a asymmetric silica exposed-core fiber; and a microscope image of (b) the cross section of a cane which was used in a two step (cane and sleeve) process to produce a asymmetric silica exposed-core fiber shown by SEM images (c); and, (d) an enlarged image of the core having an effective diameter of 1.7 μm.

(Eq. (5)) and compared to the model, since a consistent method for such a measurement could not be found and further work is needed to understood, account for, and predict such geometry changes in the draw process. Nevertheless, since the outside diameter does not contribute in the calculation of C given by the Fitt model (Eq. (7)), it was still possible to predict the pressure needed, fabricate this asymmetric structure, and create a fiber useful for the intend application [50].

The above experiment used a one step drawing process from preform to fiber. It is also common to use two steps in the drawing of fibers, in order to achieve small core sizes [49, 51], which requires the successful application of the right combination of parameters in order to achieve the desired final fiber structure. For this another preform was fabricated, as discussed above for the exposed-core fiber, and drawn down to fiber using the cane and sleeve method discussed in Sec. 3.2.1.

For the cane, we chose a feed rate of 7.5 mm/min with the targeted outside diameter for the cane being Ø2.9 mm maximum. The aim was to expand the holes slightly during the caning process, for which we chose a geometry change ratio of $C = 1.25$. Using Eq. (7) the predicted pressure (p_f) needed to achieve this was 1.64 kPa at a furnace temperature of 2000 °C. A microscope image of the resulting cane structure is shown in Fig. 5(b), which was measured as being Ø2.8 mm (measured at the maximum) with the hole region diameter Ø1.48 mm.

A sleeve was made by drilling a Ø2.9 mm hole centrally located in a Ø12 mm F300HQ silica rod and cutting a 1.8 mm wide slot along the length of the hole, into which the cane was placed ensuring that the sleeve slot lined up with the cane slot. The setup of the cane and sleeve arrangement was made to ensure that the cane would remain orientated correctly with the slot of the sleeve during drawing, as well as ensuring that pressure was only applied to the two holes of the cane. The aim was to draw down the cane and sleeve to a exposed-core fiber with a core size of Ø1.5-2.0 μm and target outside diameter of Ø150 μm. We chose a geometry change ratio of $C = 1.3$, since the holes of the cane were already expanded, for which Eq. (7) predicted the pressure (p_f) needed to achieve this was 1.80 kPa at a furnace temperature of 2000 °C and feed rate of 1.5 mm/min. A single 80 m long length of exposed-core fiber was fabricated using those parameters, as shown by the SEM images in Figs. 5(c)-5(d). This fiber outer diameter was measured using SEM images as being Ø152 μm (measured at the maximum) with the hole region diameter Ø19.1 μm. The core of this fiber, shown by the green box in Fig. 5(d), was measured as having a effective diameter of Ø1.7 μm. As discussed above, C was not calculated from measurements (Eq. (5)) and compared to the model, since this asymmetric structure no longer resembles the preform due to surface tension effects on the outside geometry.

These fabricated asymmetric exposed-core fiber structures have extremely non-

axisymmetric cross sectional wall thicknesses about the hole structure for which we use Eq. (7) to calculate the parameters. Since the Fitt model is independent of the outside diameter the parameters needed to make these structures could be predicted, within the geometry change ratio (C) limits of the types of asymmetric and symmetric multi-hole fiber structures we have shown.

4. Conclusion

The ability to predict the experimental drawing parameters needed to produce desired final MOF geometries requires a practical understanding of the draw process beyond what is achievable by trial and error. For the first time, we have described using the analytical model provided by Fitt *et al.* [26] to determine the draw conditions needed to produce multi-hole MOFs. Our results have shown that although the Fitt model describes a capillary draw process, it provides powerful and practical insights when applied to more complex multi-hole symmetric and asymmetric structures. By understanding the draw process, both in terms of the draw tower temperature profile and establishing a method to relate the geometry of a multi hole MOF to a capillary, it was found that analytical equations given by the Fitt model could predict the drawing conditions needed to produce the chosen structures.

For asymmetric structures it was found that the outside no longer resembles the preform from which it was made, due to surface tension effects. These effects add a degree of complexity not accounted for in the Fitt model or in the way the geometry is defined and further work is needed to understand and account for such geometry changes in the draw process.

Acknowledgments

This work was performed in part at the OptoFab node of the Australian National Fabrication Facility utilizing Commonwealth and South Australian State Government funding. The authors acknowledge Peter Henry for his contribution to the silica fiber drawing and the Australian Defence Science and Technology Organisation (under the Signatures, Materials and Energy Corporate Enabling Research Program) for support of the suspended and exposed core silica fiber development at The University of Adelaide. Stephen Warren-Smith acknowledges the support of an Australian Research Council Super Science Fellowship and Tanya Monro acknowledges the support of an Australian Research Council Federation Fellowship.